ACS APPLIED ENERGY MATERIALS

www.acsaem.org Article

High Conductivity in a Fluorine-Free K-Ion Polymer Electrolyte

Mennatalla Elmanzalawy, Elena Sanchez-Ahijón, Ozden Kisacik, Javier Carretero-González,* and Elizabeth Castillo-Martínez*

Cite This: *ACS Appl. Energy Mater.* 2022, 5, 9009−9019 Read Online

ACCESS | Metrics & More | Article Recommendations | Supporting Information

ABSTRACT: Solid polymer electrolytes (SPEs) could play a major role in the transition to safer and high-energy-density potassium-based batteries. However, most polymeric K-ion electrolytes are based on fluorine-containing anions and flammable organic solvents, whose safety is nowadays in question. Herein, we report a facile solvent-free synthesis of a series of several poly(ethylene oxide) (PEO)-based SPE solid solutions with $KBPh_4$ salt as potassium-ion source, including the formation of two crystalline $(PEO)_n/KBPh_4$ complexes. The ionic conductivity of these novel K-ion SPEs above and below the melting point of PEO is rationalized in light of their glass-transition temperature and chemical composition. We highlight that below the melting point of PEO, the crystalline complexes may not be intrinsically ionically conducting, but they act as ion sinks preventing the polymer cross-linking and the formation of contact ion pairs and lower the glass-transition temperature leading to a conductivity of 1.1×10^{-4} S cm^{-1} at 55 °C. A high ionic conductivity of 1.8×10^{-3} S cm^{-1} is achieved at 80 °C for the optimum $(PEO)_{30}/KBPh_4$ composition (3.2 mol % $KBPh_4$). Besides, the SPE compositions were found to be stable up to 4 V vs K^0 metal electrode at 60 °C. The $(PEO)_{30}/KBPh_4$ composite electrolyte employed in an all-solid-state symmetric cell with Prussian Blue electrodes showed reversible K^+-ion (de)intercalation, where a reversible capacity of 20 mAh g^{-1} and low voltage hysteresis were achieved for 20 cycles. Considering the material availability, ease of synthesis, and promising electrochemical properties, this work may encourage future research on fluorine-free polymer electrolytes for K-ion batteries.

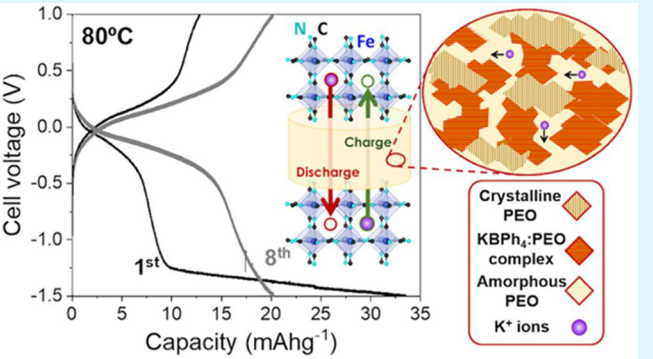

KEYWORDS: *potassium-ion battery, polymer electrolytes, solid-state battery, energy storage, electrolytes, salts*

INTRODUCTION

Lithium-ion batteries, developed to power portable electronics, are becoming increasingly deployed in electric vehicles and even larger-scale applications such as levering renewable energy storage. Nonetheless, sodium and potassium are 1000 times more abundant than lithium, and batteries based on these metals hold promise to replace LIBs for large-scale applications where the energy density is not the most important criterion and aspects such as safety, environmental friendliness, or cost become prominent. Potassium-ion batteries (KIBs) might also meet the performance requirements for transportation applications.[1] Interestingly, K^+ has faster diffusion rates than Li^+ and Na^+ in liquid electrolytes and lower desolvation energy, which result in an easier charge transfer.[2] For example, K^+ ion exhibits the highest limiting molar conductivity (15.2 S cm^2 mol^{-1}) in propylene carbonate among Li^+, Na^+, and K^+ because of the weaker Lewis acidity of K^+ ions.[2] Besides, potassium also has lower reduction electrode potential in carbonate ester solvents than lithium and sodium, enabling a large potential window of 4.6 V, and thus a plausible higher energy and power density in KIBs than in SIBs.[1] This lower plating voltage can also ensure safer batteries, as metal plating at high rates might be avoided for the same voltage window. In addition, the reversible intercalation of K^+ into graphite, the commercial anode for LIBs, with a theoretical capacity of 279 mAh g^{-1} also adds great value to KIBs.[3]

Relatively extensive research has been carried out on electrode materials, cathodes, and anodes for KIBs.[3] However, the development of rechargeable potassium batteries is hindered by the lack of safe electrolytes that not only passivate the surface of the electrode to facilitate the efficient plating/stripping of K and reversible insertion of the relatively large K^+ ions but also that enable their safe utilization.[4] Research on KIB electrolytes has been carried out using conventional electrolytes for LIBs such as carbonate and ether-derived liquid solutions, containing either potassium hexafluorophosphate (KPF_6) or potassium (fluorosulfonyl)imide (KFSI) salts.[1] However, electrolyte formulations containing dissolved fluori-

Received: May 15, 2022
Accepted: June 24, 2022
Published: July 8, 2022

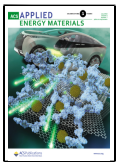

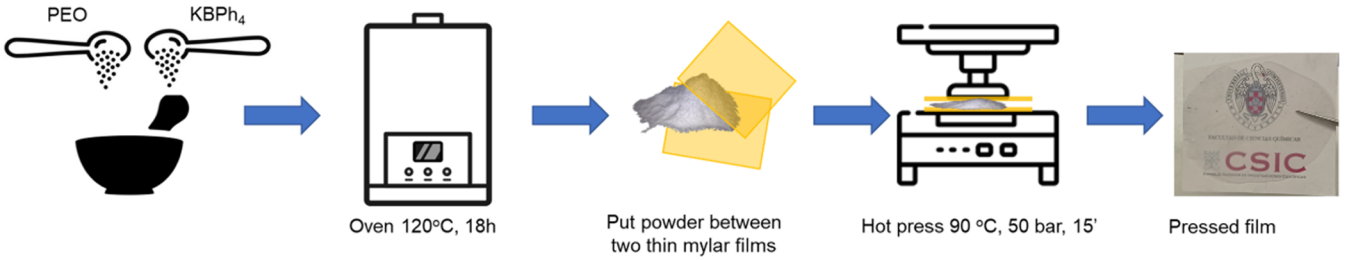

Figure 1. Schematic sequence of the synthesis route of PEO/$KBPh_4$ electrolyte films by hot pressing.

nated salts have their own issues, since flammable solvents are prone to explosion when the temperature is increased by Joule heating during a short-circuit event and, once an explosion occurs, it will result in the release of toxic fluoro-organic compounds, i.e., bis(2-fluoroethyl)-ether[5] and even hydrogen fluoride.[6] Besides these safety issues, the lower amount of fluorine atoms in the electrolyte's component is more economically favorable since the introduction of C-F bonds is energy- and resource-intensive.[7]

In 1978, Armand suggested the application of alkali metal ion-conducting polymer complexes as safe, solid electrolytes in rechargeable solid-state batteries.[8] The wide electrochemical stability window of polyethers (e.g., poly(ethylene oxide), PEO) is at least comparable to that of aprotic liquid solvents (ether, carbonates), and no co-intercalation phenomenon occurs with the inorganic host structures commonly used as electrode material. Besides, polymers are more flame-resistant than liquid electrolytes containing organic solvents, and they are, indeed, mechanically robust, lightweight, and can be shaped. A complete electrochemical screening of PEO/LiX salt complexes has been undertaken to assess their usefulness as solid-state electrolytes in rechargeable lithium-ion batteries.[9] For decades, it has been generally accepted that ionic conductivity in PEO electrolytes occurs predominantly in the amorphous phase ($T > T_g$),[10] although in the early 2000s, Bruce et al. reported ionic conductivity also in crystalline PEO−salt complexes, contradicting common belief.[11] In the amorphous phase, it is thought that ion mobility occurs through the continuous segmental motion of the polymer chains, creating new sites for ion transport and destroying the old ones.[10] Ion transport in crystalline PEO complexes however is believed to occur by hopping of the cations between sites generated by defects along the polymer tunnels, as in ionic solids.[11] The typical ionic conductivities of PEO−Li-ion salt complexes are usually below 10^{-4} S cm^{-1} at room temperature,[12] resulting mainly from the high degree of crystallinity of PEO. However, beyond the melting point of PEO crystals (~65 °C),[13] the diffusion rates of the metal alkali ions are comparable for the electrolyte and some electrode materials, achieving conductivities close to organic liquid electrolytes, thereby enabling the cycling of a solid-state cell.[6] In recent years, there have been numerous attempts to improve the performance of SPEs by hybrid electrolyte engineering,[14] the incorporation of nanofillers,[15] and the incorporation of ionic liquids[16] and quasi-ionic liquids.[17]

Although not studied for its application in rechargeable batteries, in 1973, Wright and Fenton already showed that the conductivity of a PEO−potassium thiocyanate salt (KSCN) complex was sensitive to temperature, and it increased markedly as the degree of crystallinity was reduced.[18] Since then, little research has been carried out on the development of K-ion-conducting polymer electrolytes. Among the main reasons are: (i) the procurement of carefully selected liquid phase organic electrolytes that led to the creation of the first lithium-ion "rocking-chair" cell commercialized by Sony Corporation in June 1991;[19] (ii) the weak diffusivity and poor kinetics of the K^+ ions in the solid state;[20] and (iii) although several potassium salts have shown high solubility in the most frequently used aprotic organic liquid solvents,[1] the situation differs when a solid-state polymer is used as an ionizing medium. Because of the hard basic character (Pearson theory) of halides, potassium halide salts (except KI) are neither soluble in PEO nor in other polyethers such as poly(propylene oxide) (PPO), readily recrystallizing in the form of pure alkali metal salts after mixing.[18,21] Similar behavior was also evidenced for other hard basic organic anions like carboxylates and nonperfluorinated sulfonates in PPO matrix.[15] Due to the low concentration of potassium charge carriers, the PEO-based polymer complexes containing K-metal halides and oxy-halides have shown low conductivity values at room temperature (values ranging between 10^{-7} and 10^{-8} S cm^{-1}).[22] One of the earliest works showing exceptionally high K-ion conductivity values, 2×10^{-3} S cm^{-1}, at room temperature (RT) and low activation energy (0.16 eV) deals with the formation of polymeric complexes between PEO and a potassium-silver halide salt.[23] However, the authors suggested that the high conductivity was probably due to the presence of free KAg_4I_5 salt rather than to the PEO−salt complexes.

Inherited from the Li-ion electrolytes field, potassium salts presenting low lattice energy, made of anions with highly delocalized electron density and molecular flexibility such as those based on the above-mentioned sulfonyl amide functional group, have been also implemented for the development of K-ion polymer electrolytes in gel,[24] single-ion K-ion-conducting polymer gel,[25] and solid-state electrolyte.[22] To the best of our knowledge, the successful application of a water-free K-ion polymer electrolyte in an all-solid-state half-cell has only been reported so far with a fluorine-containing salt, the KFSI. In one work, PEO-KFSI electrolyte membranes evidenced high conductivity values up to 10^{-4} S cm^{-1} at 60 °C.[26] Instead, KFSI with a matrix of poly(propylene carbonate) showed a conductivity value of up to 1.36 10^{-5} S cm^{-1} at ambient temperature.[27] Although these solid-state electrolytes are intrinsically safer than flammable liquid electrolytes, further advances could be achieved by creating highly conducting K-ion polymer electrolytes composed of fluorine-free potassium salts.

Herein, we have developed highly conducting K-ion polymer electrolytes (1.8×10^{-3} S cm^{-1} at 80 °C and 1.1×10^{-4} S cm^{-1} at 55 °C) using a scalable solvent-free process that involves the chemical reaction between PEO and a fluorine-free potassium

https://doi.org/10.1021/acsaem.2c01485
ACS Appl. Energy Mater. 2022, 5, 9009−9019

Table 1. Nomenclature of PEO/$KBPh_4$ Electrolyte Samples and Their Corresponding Molar Ratios and Concentrations

designation	PEO	PEO50	PEO37.5	PEO30	PEO25	PEO20	PEO15	PEO10	PEO8	PEO5	$KBPh_4$
molar ratio (PEO):$KBPh_4$	1:0	50:1	37.5:1	30:1	25:1	20:1	15:1	10:1	8:1	5:1	0:1
$KBPh_4$ concentration (mol %)	0	2.0	2.7	3.2	3.9	4.8	6.3	9.1	11.1	16.7	100.0

salt, potassium tetraphenylborate ($KBPh_4$), at 120 °C. The polymer electrolyte membranes were created using a mild hot-press process (90 °C, 15 min, 50 bar). The PEO/$KBPh_4$ composites contain novel crystalline phases within adducts of enhanced ionic conductivity at different temperatures depending on the composition. Therefore, the system allows the choice of the optimum composition/conductivity toward their final application. The electrolyte is capable of enabling reversible potassium-ion intercalation in a Prussian Blue symmetric cell.

EXPERIMENTAL SECTION

Synthesis of the K-Ion Polymer Electrolytes. Prior to synthesis, poly(ethylene oxide) (average $M_w \sim$ 5,000,000, Sigma-Aldrich) in powder form and potassium tetraphenylborate ($KBPh_4$ 97%, Sigma-Aldrich) were dried overnight at 55 and 120 °C, respectively, in a Buchi glass oven (B-585 model) under vacuum. The preparation of the fluorine-free PEO-based electrolyte films was done via hot pressing without the use of any liquid solvent as described in Figure 1. First, the PEO powders were gently mixed with the $KBPh_4$ salt according to the ratios described in Table 1, in an agate mortar, inside a glovebox (inert) with argon atmosphere where O_2 and H_2O concentrations were maintained below 0.1 and 0.5 ppm, respectively. The ground mixture was sealed in airtight aluminized envelopes and transferred to an oven to react at 120 °C overnight for 18 h followed by slow cooling in the oven. After the reacted blend was recovered in the glovebox, it was placed inside another sealed envelope between two thin mylar films. The envelope was then hot-pressed at 90 °C under 50 bar for 15 min and brought back into the glovebox for pressed film manipulation.

Preparation of Prussian Blue-$(PEO)_n$/$KBPh_4$ Composite Electrodes. First, a $(PEO)_n$/$KBPh_4$ binder material was prepared by mixing the proper amounts of PEO and $KBPh_4$ in a mortar inside the glovebox. The selected PEO/$KBPh_4$ ratios for the binder compositions were the same as those for PEO15 and PEO30 polymer electrolytes. Conductive carbon black (C·Energy Super C65, Imerys) and Prussian Blue (PB) (Sigma-Aldrich, microscopy purity) were next added to the binder and ground together inside an Ar-filled glovebox. Table 2 shows different proportions of the binder, conductive, and active components of the electrodes.

Table 2. Prussian Blue Composite Electrode Composition

	PEO/$KBPh_4$ mixture "binder"		Prussian Blue		Super C65	
	%	mass (g)	%	mass (g)	%	mass (g)
PB@20%PEO30	20	0.05	60	0.15	20	0.05
PB@20%PEO15	20	0.05	60	0.15	20	0.05
PB@40%PEO15	40	0.10	40	0.10	20	0.05

The resulting mixture containing PEO, $KBPh_4$, C, and PB was sealed in aluminum bags to maintain the Ar atmosphere while it is heated at 120 °C for 18 h in an oven. Then, the powder was recovered in the glovebox and placed in between two thin Mylar films and sealed in an aluminum envelope again. The envelope was then hot-pressed at 90 °C under 50 bar for 15 min. The result was a powder that was scrapped off from the thin Mylar film and recovered in a vial. Then, the electrode in powder form was added to the symmetric cells, where it was subsequently integrated as a homogeneous film after 24 h at 80 °C (Figure S1).

Structural and Thermal Characterization. Small pieces of the PEO-based polymer films were analyzed by collecting X-ray diffraction (XRD) data in the 2θ range of 5−60° in a Bruker D8 Advance diffractometer with Cu Kα radiation (λ = 1.54 Å) and a step size of 0.02° at room temperature.

Thermogravimetric analysis (TGA) was performed in a thermobalance from TA Instruments (TA-Q500 model) attached to a Pfeiffer Vacuum ThermoStar GSD 301 T mass analyzer. The gas used was nitrogen for the nonoxidant atmosphere and air for the oxidant one within a temperature interval of 25−600 °C, at a heating rate of 10 °C min^{-1} and with a sample mass of 5 mg. The results are shown in Figure S2.

The temperature and heat flow associated with thermal transitions in the polymer electrolytes were obtained using differential scanning calorimetry (DSC) performed in an equipment from Netzsch (DSC 214 polyma model). The samples were all sealed in aluminum pans. The first heating goes from room temperature to 100 °C, the temperature is held for 3 min, then scanned down to −90 °C, held for 3 min, and heated a second time up to 200 °C at a rate of 10 °C min^{-1}.

Electrochemical Characterization. All of the electrochemical characterization of the polymer electrolytes was studied in a VMP3 multichannel potentiostat/galvanostat (Bio-Logic). The ionic conductivity of the polymer electrolyte films was determined using electrochemical impedance spectroscopy (EIS). The measurements were conducted in Swagelok cells, where the electrolyte film was sandwiched between two stainless steel blocking electrodes. The temperature was controlled by placing the cell inside a Buchi glass oven (B-585 model) capped with a Teflon tap. For each of the electrode compositions, impedance plots were recorded after heating the cells at 80 °C overnight and then while cooling the cells from 80 °C to room temperature. Measurements over a frequency range 100 mHz to 1 MHz were collected after holding the cell at each temperature for 1 h for temperature stabilization (Figure S3). The Nyquist plots were interpreted using the model illustrated in Figure S3c. The conductivity's dependence on temperature was expressed by the Vogel−Tamman−Fulcher (VTF) model, which predicts that the highest conductivities will be obtained in polymers with a low T_g.[28]

A selection of those polymer electrolyte compositions showing high conductivity below and beyond the melting point of PEO crystals was tested in all-solid-state symmetric cells. Prussian Blue (PB), with ideal formula $KFe^{3+}[Fe^{II}(CN)_6]$, was the electrode material of choice for these experiments because of its ability to reversibly intercalate two K^+ ions per formula unit, equivalent to 170 mAh g^{-1} theoretical capacity.[29−31] The selected PEO/$KBPh_4$ ratios for the binder compositions were the same as those for PEO30 and PEO15 polymer electrolytes. Conductive carbon black (C·Energy Super C65, Imerys) and PB (Sigma-Aldrich, microscopy purity) were added to the binder and mixed inside an Ar-filled glovebox. Table 2 shows the electrodes with different proportions of the binder, conductive and active material components. Then, the electrode in powder form was placed into the symmetric cells, where it was subsequently integrated with the polymer electrolyte film as a homogeneous film after 24 h at 80 °C. This temperature is the same needed to achieve a hold temperature to run the galvanostatic discharge and charge measurements. The cycling performance of the all-solid-state potassium-ion battery at 80 °C was acquired at 0.085, 0.042, 0.0085, and 0.0042 mA cm^{-2} current densities with a cutoff voltage of −1.5 to 1 V.

Finally, the solid polymer electrolyte was also tested by linear sweep voltammetry (LSV) to determine the voltage stability window at the blocking (stainless steel) and nonblocking (PB) electrode materials. Cells containing potassium metal were stabilized and measured at 60 °C, while those with PB were stabilized and measured

https://doi.org/10.1021/acsaem.2c01485
ACS Appl. Energy Mater. 2022, 5, 9009−9019

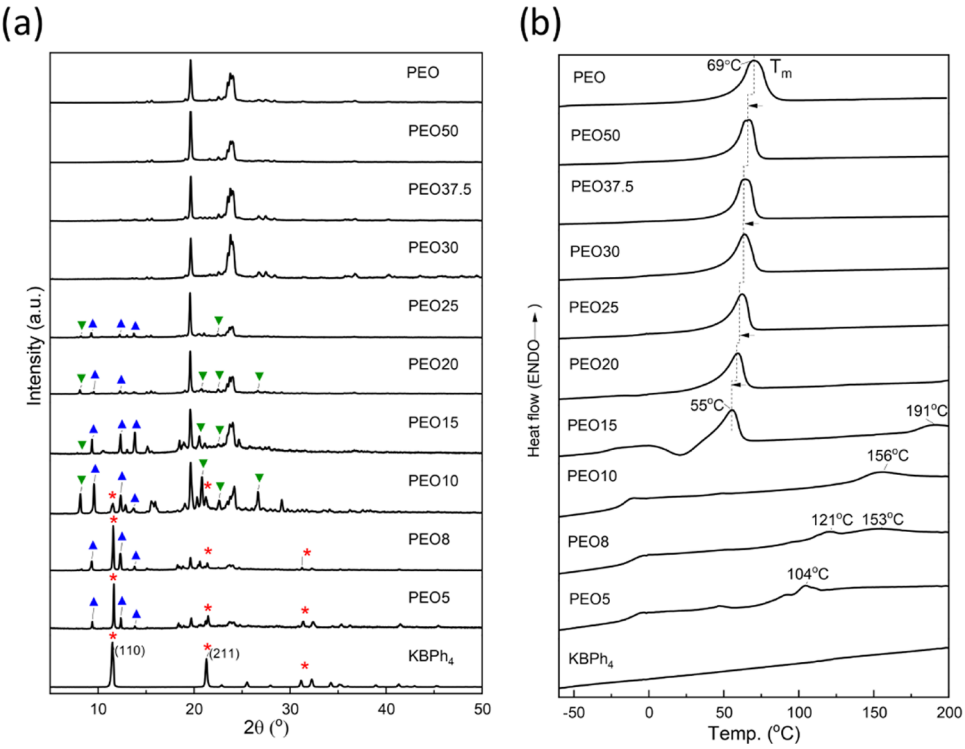

Figure 2. (a) XRD patterns of $(PEO)_n$–$KBPh_4$ composites. Blue triangle up solid: salt-rich complex 1, green triangle down solid: Salt-rich complex 2, red star: $KBPh_4$. (b) DSC second heating curves for PEO-$KBPh_4$ composites.

at 80 °C. Because potassium melts at 63 °C,[32] pure potassium metal was avoided as counter electrode when measuring at 80 °C. A blocking stainless steel current collector was used in the latter case. The LSV curves were obtained at a 1 mV s^{-1} scan rate from OCV to 6 V vs E_{Ref}.

RESULTS AND DISCUSSION

The preparation of highly conducting K-ion solid polymer electrolyte was achieved by simple mixing, heating, and pressing protocol described in the Experimental Section. After synthesis, the polymer–salt composites in film form with an average thickness of ∼200 μm were ready to be cut into pieces for their characterization or into disks to be studied and used as K-ion polymer electrolytes. XRD patterns of the polymer/salt complexes were recorded as depicted in Figure 2a. Diffraction peaks corresponding to free $KBPh_4$ salt (highlighted with a red star symbol), namely, at 2θ angles of 11, 21, 31, and 32°, remain present in the samples with higher salt contents, from PEO10 to PEO5. The most intense (110) reflection of free $KBPh_4$ becomes narrower in the salt-rich samples than in the pure salt, which suggests an increase in the $KBPh_4$ crystal size due to hot pressing.

On the other end, all of the PEO-rich samples retain the reflections of crystalline PEO, with no change in lattice parameters suggesting that the salt is mostly diluted within the amorphous PEO regions. Meanwhile, as the ratio of salt increases from pure PEO, starting from PEO25 and higher salt samples, the most intense reflections corresponding to crystalline monoclinic PEO decrease in intensity, along with the appearance of new diffraction peaks. This result points to a decrease in the content of crystalline PEO with the addition of salt, a consequence of complexation between $KBPh_4$ and PEO, giving rise to new crystalline phases and amorphous salt/PEO domains. Such amorphization, as a result of salt complexation, has been previously reported in earlier studies, where it was revealed that complexation happens through an interaction between the oxygen atoms of the ethoxy groups and the cations, in this case potassium.[18] Notably, new diffraction peaks, namely, at 2θ values of 9, 12, and 14°, appear in the salt-rich compositions from PEO25 to PEO5, indicating the formation of a new crystalline phase aside from the PEO and $KBPh_4$ crystals (referred to as salt-rich complex 1 in Figure 2a). A few samples, PEO10, PEO15, and to some degree PEO20, exhibit unique diffraction peaks at 8° and around 20° (referred to as salt-rich complex 2). The origin of these peaks could be attributed to either a second salt-rich complex phase, or alternatively a superstructure of the first salt-rich phase; however, the difficulties to grow crystals for any composition and the absence of a crystal structure for complex 1 prevented us from elucidating this.

The decrease of crystalline phases along with the increase of salt content detected by PXRD is further confirmed by differential scanning calorimetry (DSC). DSC second heating curves for the hot-pressed electrolyte samples are shown in Figure 2b and enlarged in Figure S4. A consistent decrease in the melting point of crystalline PEO is observed as salt content increases, from 69 °C in pure PEO to 55 °C in PEO15, which appears after an exothermic peak due to crystallization for this composition suggesting slow kinetics of crystallization. However, the PEO melting peak on the second heating largely decreases to 49 °C for PEO10 and disappears at higher salt concentrations starting from PEO10 onwards, indicating very little or negligible crystalline PEO content in these compositions (see Supporting Information Figure S5 for further discussion and first heating data). Melting point depression is expected in miscible systems. The melting point of a chain polymer depends on the average molecular cohesion energy, and that is heavily influenced by molecular flexibility.[33]

https://doi.org/10.1021/acsaem.2c01485
ACS Appl. Energy Mater. 2022, 5, 9009–9019

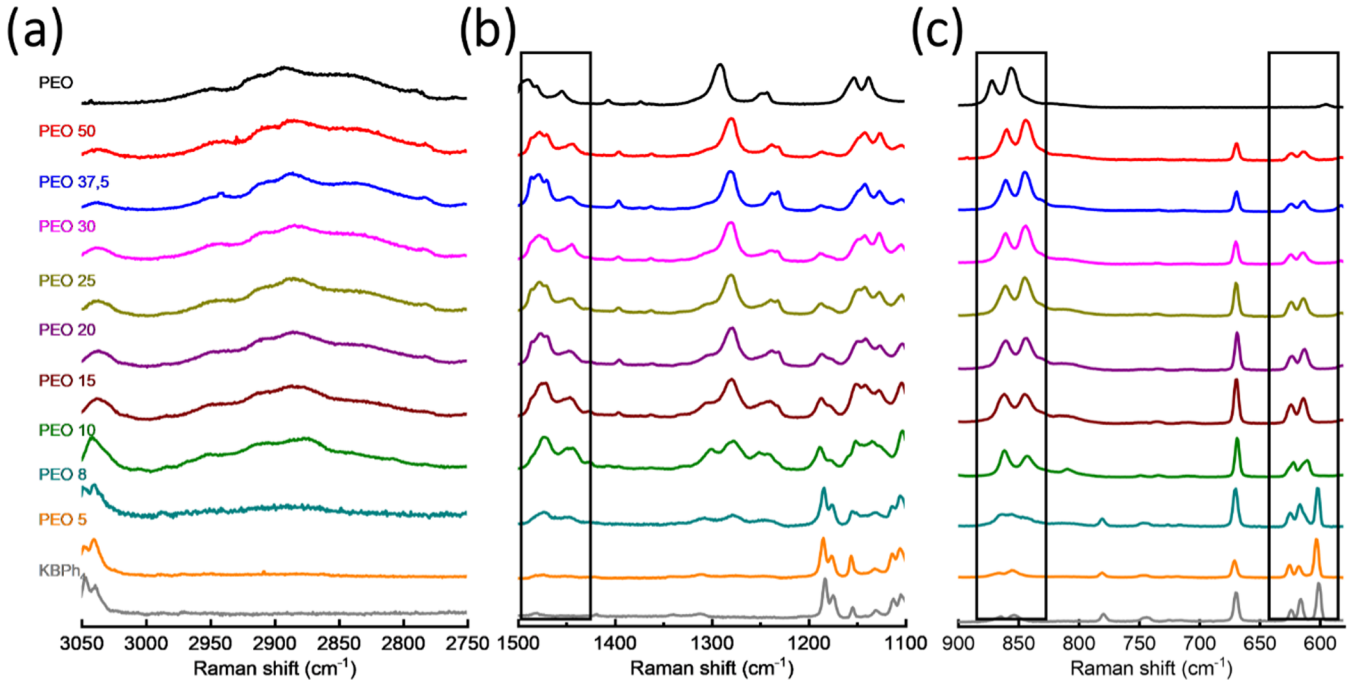

Figure 3. Raman spectra of PEO/$KBPh_4$ samples in the wavenumber ranges of (a) 3050−2750 cm^{-1}, (b) 1500−1100 cm^{-1}, and (c) 900−580 cm^{-1}.

It is then no surprise that T_m and T_g in semicrystalline polymers are usually correlated.[34]

At higher salt concentrations, broad endothermic peaks appear at higher temperatures above 100 °C, most likely corresponding to the melting of the polymer−salt crystalline complexes detected by PXRD. In PEO15, a broad peak appears at 191 °C. The crystalline complex contributing to this peak does not appear for any other composition at temperatures below 200 °C. In PEO10 and PEO8, broad melting points at 156 and 153 °C appear, respectively. The new melting points correspond to the melting of a different phase than that appearing at PEO15. Moreover, broad melting peaks appear for PEO8 and PEO5 at 121 and 104 °C, respectively. There is no evidence from XRD data to suggest that these peaks belong to a third crystalline phase; thus, it is reasonable to assume that they belong to the melting of a mixture of two crystalline PEO−salt complexes. A gradual decrease in the enthalpy of melting of the PEO crystals with the increase of salt concentration indicates a decrease in the ratio of crystalline to amorphous PEO—a natural consequence of the salt acting as a diluent for the polyether, in agreement with the Flory−Huggins theory.[35] In summary, analysis of the XRD patterns, coupled with DSC results, suggests the formation of two different crystalline PEO/$KBPh_4$ complexes at high salt concentrations and a decrease in the total crystalline PEO content.

Since the $KBPh_4$ salt is dissolved in different amorphous and crystalline phases, the ethoxy groups around it are expected to have different conformations in each of them. The study of the vibrational spectra of polymer electrolytes is a powerful tool to explore conformational changes that occur at various salt contents. Raman spectra of the polymer electrolyte composites, as well as the pure salt and PEO, are displayed in Figure 3.

First of all, upon addition of a small amount of salt to PEO there is a notable shift of most crystalline PEO peaks to lower wavenumbers, suggesting the bulk complexation of the salt by PEO. Upon increasing the $KBPh_4$ content, the methylene stretching (3000−2750 cm^{-1}, Figure 3a), bending (1500−1400 cm^{-1}, Figure 3b), and rocking (900 and 800 cm^{-1}, Figure 3c) bands all decrease in intensity, suggesting the transition of PEO into a less ordered state.[36] This agrees with the DSC and XRD results discussed in previous sections.

The study of vibration bands of the anions in particular can give information on the possible formation of ion pairs or higher aggregates. Three peaks, namely, at 601, 616, and 624 cm^{-1}, are assigned to the anion $(BPh_4)^-$[37]. Notably, the peak at 601 cm^{-1} was assigned to B−Ph stretching vibration, which remains in the pure salt, PEO8 and PEO5, confirming that free salt anions are present in higher salt compositions, as detected by XRD.[37] The peak at 616 cm^{-1} is assigned to in-plane ring deformation, and the one at 624 cm^{-1} is assigned to an ionic lattice vibration.[38] The intensity of both peaks decreases gradually in samples of lower salt content. Since the anions are only weakly interacting with the polymer chains in salt-polymer complexes, perturbations of the B−Ph_4 stretching vibration modes could be indicative of anions pairing with cations.[39] The coordination of K^+ cations to the BPh_4^- anions disturbs the symmetry of the BPh_4^- molecule, as indicated by the shift of the 616 and 624 cm^{-1} peaks. This shift is largest for the PEO10 composition, indicating a different kind of ion−ion coordination and possibly the formation of contact ion pairs.

The most important parameter for the application of this PEO-$KBPh_4$ system as electrolyte in KIBs is its ionic conductivity. Arrhenius plots of the polymer electrolyte composites with different salt concentration are shown in Figure 4a. As shown by eq S2, salt concentration and ionic mobility have a direct impact on the value of ionic conductivity; the latter is evidenced by the presence of two main linear regions in the $\log(\sigma)$ vs $1/T$ plot for most of the compositions, one below and the other above the melting point of PEO crystals. Thus, the composite with the highest salt content is not the one with the highest conductivity. In the

https://doi.org/10.1021/acsaem.2c01485
ACS Appl. Energy Mater. 2022, 5, 9009−9019

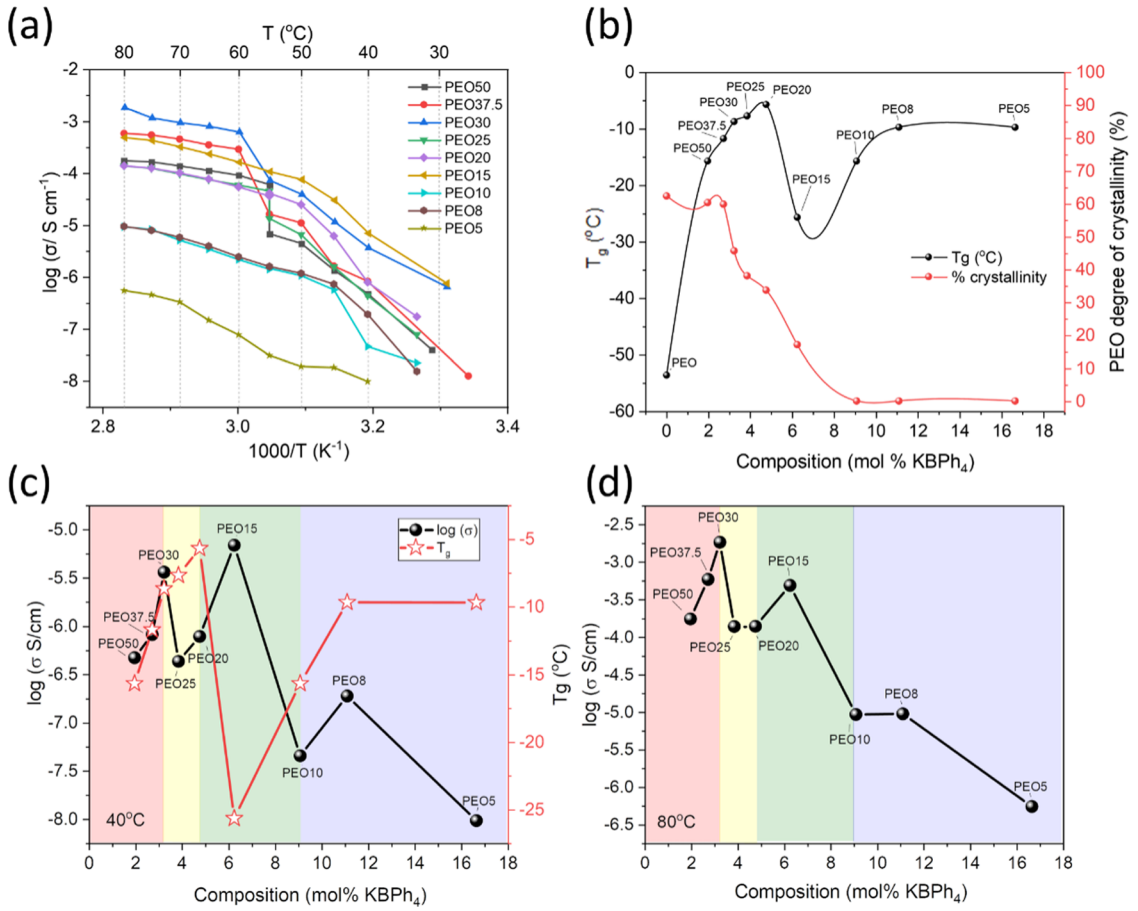

Figure 4. (a) Arrhenius plots for all of the polymer/salt composite electrolytes included in this work. (b) Glass-transition temperature and degree of crystallinity evolution with salt concentration. Curves are drawn using a cubic spline function as a guide to the eye. (c, d) Isotherms of ionic conductivity vs mole fraction of $KBPh_4$ in the polymer electrolyte at (c) below (40 °C), and (d) above (80 °C) the melting point of crystalline PEO. T_g values are plotted in the secondary *y*-axis of (c).

high-temperature regime, PEO30 showed the highest conductivity (1.8×10^{-3} S cm^{-1} at 80 °C), despite having one of the lowest salt concentrations; meanwhile, in the low-temperature regime below the melting range of PEO, PEO15 was superior (1.06×10^{-4} S cm^{-1} at 55 °C and 7.43×10^{-7} S cm^{-1} at ambient temperature, 25 °C). The salt concentration will also influence the presence of crystalline/disordered PEO and the formation of different PEO−salt complexes having both a direct impact in the ionic mobility (because of the actual changes in salt concentration at the amorphous PEO) as confirmed by PXRD, DSC, and Raman techniques.

To shed light on the possible reasons behind the correlation between conductivity and electrolyte composition, we analyzed both glass-transition temperatures and the degree of crystallinity trends for the different K-ion polymer electrolyte compositions under study (Figure 4b). The degree of crystallinity of PEO (calculated from the integral of the melting peak in the DSC) and the T_g of each sample are also reported in Table S1. Figure 4b evidences a rapid increase of T_g from −53 °C in pure PEO to −16 °C upon addition of a small amount of salt (2 mol %) in PEO50. Initially, an increase in T_g is observed as the amount of salt increases. An increase in glass-transition temperature is not desired for an ionically conductive polymer as it limits the segmental motion and thereby is expected to decrease the conductivity under ambient conditions. This is typical for polymer electrolyte systems, where a transient cross-linking of the polymer chains occurs due to the interaction between the polymer and the salt. However, at higher salt concentrations (starting at PEO15), T_g suddenly decreases, indicating an improvement in the mobility of the polymer backbone for the PEO15 electrolyte. This could be explained by the increased electrostatic repulsion between anions at higher salt contents,[40] in addition to the formation of ion aggregates, decreasing the interaction between the polymer chains and the salt.[41] One could argue that because of the formation of crystalline complexes as detected by XRD, the concentration of salt in the remaining free PEO is effectively lower and the cross-linking effects are suppressed, as seen in Figure 4b. Hence, polymer−salt complexes are acting as ion sinks consuming the ions that would have otherwise contributed to cross-linking and higher T_g. Indeed, apart from pure PEO, the lowest glass-transition temperature is for PEO15 polymer electrolyte, lower than that of PEO-rich compositions. This reflects that there is an increased chain mobility at this special composition due to phase mixing. Hence, one can predict an improved ionic conductivity for this sample at temperatures below the melting point, as it will be discussed next.

Ionic Conductivity below the Melting Point of the PEO Polymer Matrix. The conductivity behavior in the two distinct regimes can be better understood by looking in more detail at the evolution of the conductivity with the composition in each regime: below (Figure 4c) and above (Figure 4d) the melting point of the crystalline phase of the PEO matrix. In the

https://doi.org/10.1021/acsaem.2c01485
ACS Appl. Energy Mater. 2022, 5, 9009−9019

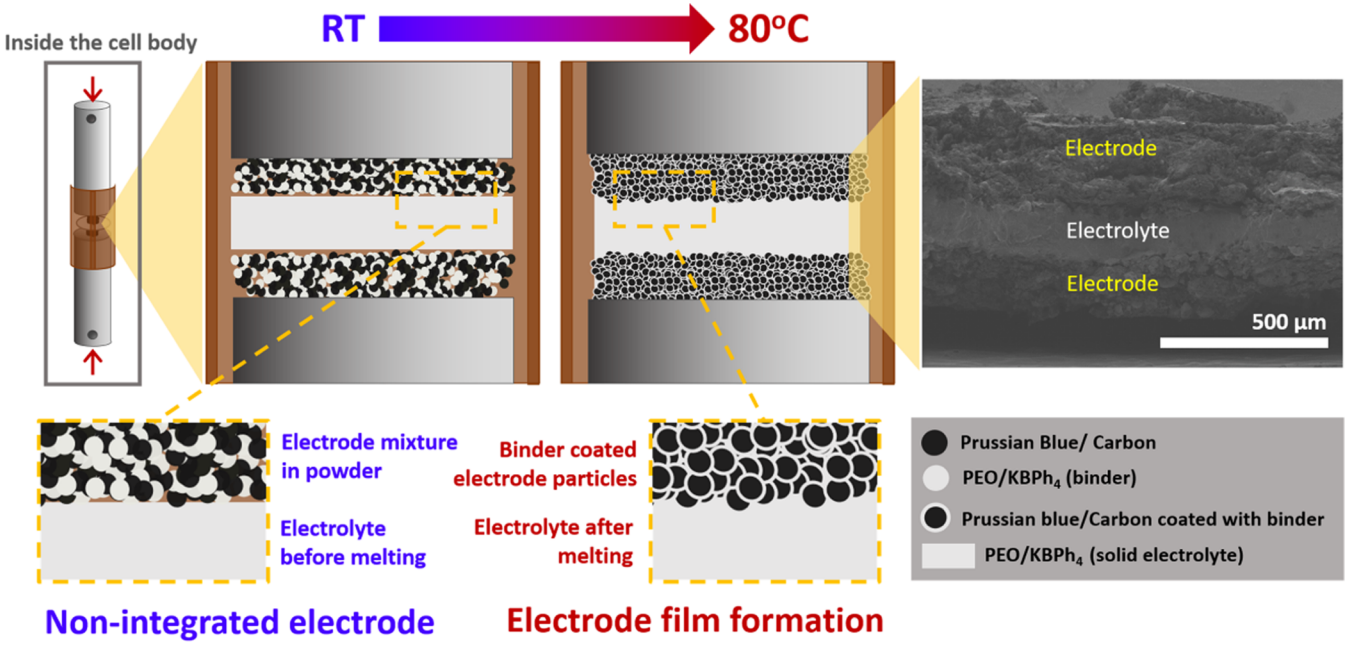

Figure 5. Graphical scheme of the electrode film formation and integration with the electrolyte during cell heating, with SEM image of the cell cross section showing the electrode/electrolyte/electrode layers after cycling.

case of the low-temperature regime (Figure 4c), the glass-transition temperature is an important parameter to consider as it often implies the polymer's chain mobility. As it was inferred from the discussion of Figure 4a,b, a low T_g is desirable because it implies high ionic conductivity. For instance, Figure 4c confirms that at PEO15, where T_g is at a minimum, the conductivity is higher than in any other composition studied herein.

Figure 4c describes the relationship between ionic conductivity, salt concentration, and T_g at 40 °C, and can be divided into four regions. In the red region (PEO−PEO30), an increase in salt concentration leads to an increase in the number of charge carriers, hence the gradual increase in conductivity from PEO50 to PEO30. But, since T_g also increases with the addition of salt as a consequence of the increase in the number of transient cross-links in the bulk polymer,[42] it starts to limit the chain mobility, hence limiting ionic conductivity as shown in the yellow region (PEO30−PEO20).

As the salt content increases further (green region, PEO20−PEO10), T_g suddenly decreases, reaching a minimum of −26 °C at PEO15, giving rise to the highest conductivity (6.8×10^{-6} S cm $^{-1}$) shown in the green region, measured at any temperature up to 55 °C (Figures 4c and S6). The decrease in T_g value could be the result of the dilution of the ionic interaction between the ions of the salt and the PEO backbone in the crystalline and amorphous PEO in the presence of the newly formed crystalline PEO/$KBPh_4$ complexes. This phase coexistence leads to a decrease in melting temperature. Afterward, any further addition of salt contributes to two competing effects. On the one hand, the addition of salt decreases the degree of PEO crystallinity, in principle increasing conductivity, but on the other hand, it also contributes to an increase in ion aggregates and the formation of even more PEO/$KBPh_4$ rigid crystalline complexes as seen by the DSC, XRD, and Raman measurements, where crystalline PEO−salt complexes are prominent with increasing salt contents. The latter effect dominates, limiting the conductivity in the blue region (PEO10−PEO5). Interestingly, although PEO8 and PEO5 have similar T_g and degree of crystallinity, there is a large difference in their ionic conductivity values. This could be explained in light of the existing competition between the crystalline complexes and the formation of ion pairs. We have established that the formation of PEO/$KBPh_4$ complexes that act as ion sinks can hinder the formation of ion pairs. However, once the composite is "saturated" with these complexes, any further addition of salt would only contribute to the formation of more ion pairs and aggregates, therefore decreasing the ionic conductivity. One can speculate that this saturation happens at compositions somewhere between PEO8 and PEO5.

Ionic Conductivity above the Melting Point of the PEO Polymer Matrix. The relationship between the concentration of salt and the ionic conductivity above the melting point of crystalline PEO, at 80 °C is displayed in the isotherm of Figure 4d. At this temperature, ionic conductivity primarily occurs in the amorphous phase and it is highly affected by the increase of salt content[43] and less affected by the T_g. In the red region, an increase in charge carrier concentration correlates to an increase in conductivity, reaching a maximum at PEO30 (1.8×10^{-3} S cm^{-1}). The conductivity decreases again in the yellow region, where ion pair formation likely takes place. New crystalline PEO/$KBPh_4$ complexes start to form in the green region, consuming the ion pairs and giving rise to high conductivity again, reaching 4.9×10^{-4} S cm^{-1} at 75 °C for PEO15. However, the complexes retain high salt concentration at 75 °C (Figures S6 and 2b) and do not contribute to the ionic conductivity as much as the molten PEO−salt matrix. Finally, in the blue region, any further addition of salt consumes free PEO and increases ion pair formation as detected at room temperature by Raman spectroscopy (Figure 3).

All-Solid-State Potassium-Ion Symmetric Cell. The two compositions showing the highest ionic conductivities

https://doi.org/10.1021/acsaem.2c01485
ACS Appl. Energy Mater. 2022, 5, 9009−9019

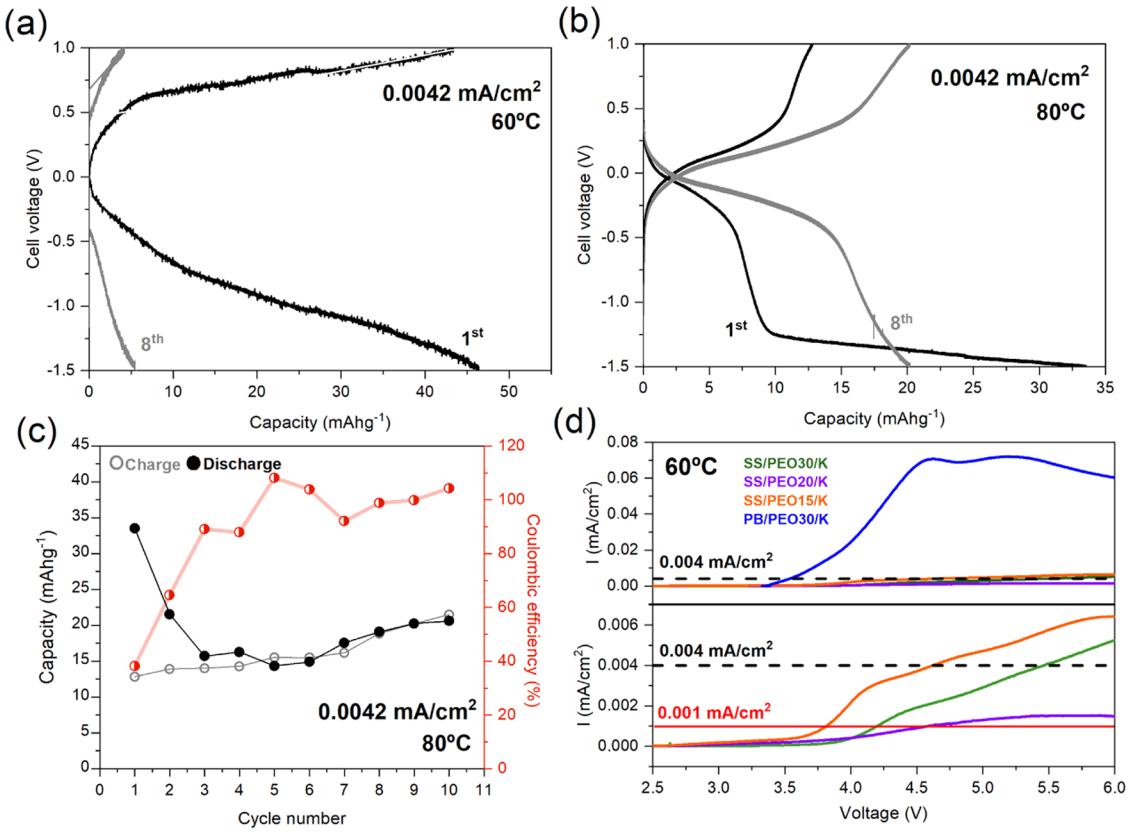

Figure 6. (a, b) Charge−discharge curves for the first and eighth cycles at 0.0042 mA cm^{-2} rate from the galvanostatic cycling of a symmetric cell where the composition PEO30 is used as electrolyte and the electrode composition is PB/C/PEO30 (60:20:20) (see Table 2 for detailed electrode composition): (a) for 60 °C and (b) for 80 °C. (c) Charge capacity (empty circles), discharge capacity (full circles), and coulombic efficiency (mid-full circles) along the cycles of the symmetric cell measured at 80 °C and rate of 0.0042 mA cm^{-2}. (d) LSV of asymmetric cells with stainless steel and potassium metal as electrodes and different PEO/$KBPh_4$ compositions as electrolyte along with PB@20%$PEO30_{(WE)}$|PEO30|$K_{(RE)}$ asymmetric cell, all measured at 60 °C. As a guide for the reader, a red dashed line chosen by the authors indicated the current density limit value (0.001 mA cm^{-2}) when the polymer electrolyte degradation might start. The black dashed line indicates the current density value (0.004 mA cm^{-2}) used during the galvanostatic charge and discharge measurements shown in (a) and (b).

beyond and below the melting point of PEO crystal (Figure 4a), PEO30 and PEO15, respectively, were chosen to build all-solid-state symmetric cells with electrodes made of commercial Prussian Blue (PB). These $(PEO)_n/KBPh_4$ composites (n = 30, 15) were used as electrolytes in Swagelok cells to test their stability, reversibility, rate capability, and long-term performance in a safer all-solid-state potassium-ion cell. To improve interfacial charge transfer and integrate the solid polymer electrolyte in the cell, polymer electrolyte compositions of PEO15 and PEO30 were also used as binder materials in both PB electrodes. XRD patterns of the electrode mixtures (PB + Carbon + PEO30) after heat treatment and hot pressing agree with the in situ formation of the binder of compositions PEO30 or PEO15 without compromising the structural integrity of PB, as shown in Figure S7.

The electrolyte and electrode integration process in the symmetric cells is shown in Figure 5. At room temperature (RT), the electrode mixture that is still in powder form exhibits an irregular and nonintegrated interface with the solid PEO30 film. However, when heated up to 80 °C for electrochemical measurements, the PEO30 "binder" of the electrode mixture and the PEO30 electrolyte become soft, forming a homogeneous electrode, with a well-integrated interface between the polymer electrolyte and the electrode. This was confirmed by the scanning electron microscopy (SEM) images of the cross section of the electrode/electrolyte/electrode assembly after cycling (Figure 5), where a good adhesion between the electrode and electrolyte is apparent.

Going beyond the melting temperature of crystalline PEO during the film formation presents some problems on the cells, which made some of them difficult to cycle. The pressure of the electrodes on the molten polymer electrolyte must be homogeneous throughout the electrode surface area to preserve the electrolyte inside the cell as much as possible (Figure S1b). Otherwise, the electrolyte flows out of the electrode area and toward the inner part in between the current collector and the Swagelok cell's body (Figure S1a), and the cell is short-circuited. These two situations are sketched in Figure S1.

After studying different electrode compositions (see Table 2), whose galvanostatic charge and discharge curves are compared in Figure S8, the cell named PB@20%PEO30, which employed PEO30 as both polymeric binder and electrolyte material, was selected because of its electrochemical performance at 80 °C. As shown in Figure 6a, the PB symmetric cell with the PEO30 electrolyte and electrode binder shows a reversible capacity of 45 mAh g^{-1} at 60 °C in the first cycle at 0.0042 mA cm^{-2}. Increasing the temperature to 80 °C (Figure 6b) largely decreases voltage hysteresis in agreement with the increase of ionic conductivity, but it also decreases the maximum reversible capacity that reaches 20 mAh g^{-1} at cycle 8. Although the full symmetric cell presents ∼64%

https://doi.org/10.1021/acsaem.2c01485
ACS Appl. Energy Mater. 2022, 5, 9009−9019

irreversibility in the first discharge due to additional redox processes occurring between +1.0 and −1.5 V, it is almost fully reversible from the sixth cycle forward. Therefore, the electrolyte composition PEO30 can transport K^+ ions back and forth between two PB electrodes (Figure 6c).

As the cell is symmetric, the main redox processes seen between −0.5 and 0.5 V relate to the simultaneous reduction and oxidation of Prussian Blue, taking place one on each electrode of the cell. The simplified ideal PB structure ($KFe^{3+}[Fe^{II}(CN)_6]$) contains two iron species in two different oxidation states.[31] The oxidation of Prussian Blue to Berlin Green ($Fe^{3+}[Fe^{III}(CN)_6]$) usually takes place at voltages around 4 V vs K^+/K,[30] while the reduction of Prussian Blue to Prussian White ($K_2Fe^{2+}[Fe^{II}(CN)_6]$) happens at voltages near 3.5 V vs K^+/K.[44] Therefore, with the cell first discharge, Berlin Green (fully depotassiated species) should form in one electrode and Prussian White (fully potassiated species) in the other.

The cyclability of the symmetric cell is shown in Figure 6c. The coulombic efficiency of the cell improves with cycling as the irreversible additional processes of the first cycle disappear; however, as we will see next, we are cycling out of the stability window of the electrolyte. After a few cycles, the reversible capacity remains stable around 20 mAh g^{-1} and increasing. This is far from the 50 mAh g^{-1} achieved for the same symmetric cell with liquid electrolyte (Figure S9b), but these are unoptimized electrode formulations and processing, and optimizing them is out of the scope of this work. From these results, we can confirm that PEO30 can function as a solid electrolyte in an all-integrated-solid-state potassium-ion cell.

The voltage stability window of the solid polymer electrolyte was studied by LSV. Figure 6d shows a comparison of the LSV profiles of three electrolyte compositions with different ratios of $(PEO)_n/KBPh_4$ versus metallic potassium. To avoid melting the potassium metal, these experiments were performed at 60 °C. Low-current-density (0.001 mA cm^{-2}) oxidation processes are detected at potentials between 3.8 and 4.4 V vs K^+/K in all cases. Commonly, PEO-based electrolytes suffer from oxidative decomposition above 3.9 V vs K^+/K due to the presence of C−O bonds that are electrochemically liable.[42] Based on the low maximum current densities achieved during the oxidation processes of the polymer electrolytes, the three polymer electrolyte compositions seem to be electrochemically stable until at least 3.8 V vs K^+/K. Beyond that voltage, they suffer minor oxidation processes at 60 °C. Nonetheless, a dependence of the stability with the $KBPh_4$ content is detected. Between 2.5 V vs K^+/K and 4.0 V vs K^+/K, the stability decreases gradually when the salt content increases from PEO30 to PEO15 as deduced from their increasing slope and current values in that voltage range. This lower reactivity for PEO30, together with its higher ionic conductivity at 80 °C, explains why symmetric cells with PEO30 as electrolyte show better electrochemical performance than those with PEO15 at 80 °C (Figure S8). Moreover, the fact that all electrolytes showed some redox processes above 3.8 V vs K^+/K (Figure 6d) also justifies that the coulombic efficiency is not closer to 100% in the symmetric PB cells (Figure 6c), and even more because PB seems to enhance the electrolyte decomposition (see Figure S10a). Despite the electrolyte decomposition taking place at voltages of PB to BG oxidation, the experiments above have allowed demonstrating the ability of the $(PEO)_n/KBPh_4$ electrolyte to transfer potassium ions back and forth between the two electrodes and opens the field to testing this family of fluorine-free solid-state electrolytes with other lower-voltage cathode materials to enable safe solid-state potassium-ion batteries.

CONCLUSIONS

$(PEO)_n/KBPh_4$ ($50 \geq n \geq 5$) polymer electrolyte films were synthesized via a solvent-free hot pressing route. In the compositional range $25 \geq n \geq 5$, the formation of crystalline $(PEO)_n/KBPh_4$ complexes was confirmed by XRD and DSC. Although these crystalline complexes do not seem to intrinsically contribute to the ionic conductivity, their existence acts as ion sinks, hindering ionic pair formation on the matrix and lowering the T_g, and thus it leads to increased ionic conductivity below the melting point of PEO, with a maximum of 1.1×10^{-4} S cm^{-1} for PEO15 at 60 °C. Above the melting point of PEO, however, when the chemical composition and structure of the composite become more homogeneous, the number of cross-links increases for the salt-rich samples, and at 80 °C, the maximum conductivity is achieved for polymer-rich PEO30 with a value as high as 1.8×10^{-3} S cm^{-1}. Our findings highlight the parameters affecting ionic conductivity both above and below the melting point of the crystalline PEO domains.

In addition to acting as electrolytes, $PEO/KBPh_4$ composites were incorporated as binder materials for Prussian Blue electrodes. In situ formation of the electrode films was performed after cell assembly and cycling of symmetric Prussian Blue cells with PEO30 electrolytes were shown plausible, enabling a reversible capacity of up to 20 mAh g^{-1} at 80 °C and 45 mAh g^{-1} at 60 °C with a large overpotential. The composite electrolyte with the highest ionic conductivity at 80 °C, PEO30, also showed the highest electrochemical stability up to 4 V vs K^+/K. To finalize, this work sheds light on the significance of structure−property relationships in polymer electrolytes design for we have shown how the structural components of a polymer composite govern its conductivity.

ASSOCIATED CONTENT

Supporting Information

The Supporting Information is available free of charge at https://pubs.acs.org/doi/10.1021/acsaem.2c01485.

Additional experimental details, including the in situ building of the symmetric cells, thermal properties of the polymer samples, conductivity behavior at all temperatures of measurement, and further tests (PDF)

AUTHOR INFORMATION

Corresponding Authors

Javier Carretero-González − *Institute of Polymer Science and Technology, ICTP-CSIC, Madrid 28006, Spain;* orcid.org/0000-0002-8008-5715; Email: jcarretero@ictp.csic.es

Elizabeth Castillo-Martínez − *Department of Inorganic Chemistry, Universidad Complutense de Madrid, Madrid 28040, Spain;* orcid.org/0000-0002-8577-9572; Email: ecastill@ucm.es

Authors

Mennatalla Elmanzalawy − *Institute of Polymer Science and Technology, ICTP-CSIC, Madrid 28006, Spain;* Present Address: Helmholtz Institute Ulm (HIU), Helmholtzstrasse 11, 89081 Ulm, Germany and Karlsruhe

https://doi.org/10.1021/acsaem.2c01485
ACS Appl. Energy Mater. 2022, 5, 9009−9019

Institute of Technology (KIT), P.O. Box 3640, 76021 Karlsruhe, Germany
Elena Sanchez-Ahijón − *Department of Inorganic Chemistry, Universidad Complutense de Madrid, Madrid 28040, Spain*
Ozden Kisacik − *Institute of Polymer Science and Technology, ICTP-CSIC, Madrid 28006, Spain*

Complete contact information is available at: https://pubs.acs.org/10.1021/acsaem.2c01485

Author Contributions

The manuscript was written through contributions of all authors. All authors have given approval to the final version of the manuscript.

Funding

The authors acknowledge financial support from the Ministry of Science and Innovation of Spain (ANOKIB; RTI2018-094550-A-I00). J.C.-G. acknowledges support from the Spanish Ministry of Economy, Industry, and Competitiveness (MINECO) through a Ramon y Cajal Fellowship (RYC-2015-17722). O.K. acknowledges support from the Erasmus+ grant through Eskisehir Technical University. M.E. acknowledges financial support from the Erasmus+ grant for mobility through the Université de Picardie Jules Verne and the Erasmus Mundus Program "MESC+" of the European Commission.

Notes

The authors declare no competing financial interest.

■ ACKNOWLEDGMENTS

The authors acknowledge technical help from Sergio González Tomé for DSC measurements. The personnel of the ICTP's characterization service: Isabel Muñoz Ochando for Raman measurements, Pedro González Pérez for XRD data collection, José David Gomez Varga for SEM, and Esperanza Benito Cano for TGA measurements, as well as the technical service from Emilio Matesanz from the X-ray diffraction Centre for Research support at UCM.

■ REFERENCES

(1) Hosaka, T.; Kubota, K.; Hameed, A. S.; Komaba, S. Research Development on K-Ion Batteries. *Chem. Rev.* **2020**, *120*, 6358−6466.
(2) Okoshi, M.; Yamada, Y.; Komaba, S.; Yamada, A.; Nakai, H. Theoretical Analysis of Interactions between Potassium Ions and Organic Electrolyte Solvents: A Comparison with Lithium, Sodium, and Magnesium Ions. *J. Electrochem. Soc.* **2017**, *164*, A54−A60.
(3) Kubota, K.; Dahbi, M.; Hosaka, T.; Kumakura, S.; Komaba, S. Towards K-Ion and Na-Ion Batteries as "Beyond Li-Ion". *Chem. Rec.* **2018**, *18*, 459−479.
(4) Liu, S.; Mao, J.; Zhang, Q.; Wang, Z.; Pang, W. K.; Zhang, L.; Du, A.; Sencadas, V.; Zhang, W.; Guo, Z. An Intrinsically Non-flammable Electrolyte for High-Performance Potassium Batteries. *Angew. Chem.* **2020**, *132*, 3667−3673.
(5) Hammami, A.; Raymond, N.; Armand, M. Runaway Risk of Forming Toxic Compounds. *Nature* **2003**, *424*, 635−636.
(6) Eshetu, G. G.; Bertrand, J. P.; Lecocq, A.; Grugeon, S.; Laruelle, S.; Armand, M.; Marlair, G. Fire Behavior of Carbonates-Based Electrolytes Used in Li-Ion Rechargeable Batteries with a Focus on the Role of the LiPF6 and LiFSI Salts. *J. Power Sources* **2014**, *269*, 804−811.
(7) Conte, L.; Gambaretto, G. P.; Caporiccio, G.; Alessandrini, F.; Passerini, S. Perfluoroalkanesulfonylimides and Their Lithium Salts: Synthesis and Characterisation of Intermediates and Target Compounds. *J. Fluorine Chem.* **2004**, *125*, 243−252.
(8) Armand, M.; Chabagno, J.; Duclot, M. *Second International Meeting on Solid Electrolytes*; St Andrews: Scotland, 1978; pp 20−22.
(9) Armand, M. The History of Polymer Electrolytes. *Solid State Ionics* **1994**, *69*, 309−319.
(10) Golodnitsky, D.; Strauss, E.; Peled, E.; Greenbaum, S. Review−On Order and Disorder in Polymer Electrolytes. *J. Electrochem. Soc.* **2015**, *162*, A2551−A2566.
(11) Gadjourova, Z.; Andreev, Y. G.; Tunstall, D. P.; Bruce, P. G. Ionic Conductivity in Crystalline Polymer Electrolytes. *Nature* **2001**, *412*, 520−523.
(12) Xue, Z.; He, D.; Xie, X. Poly(Ethylene Oxide)-Based Electrolytes for Lithium-Ion Batteries. *J. Mater. Chem. A* **2015**, *3*, 19218−19253.
(13) Money, B. K.; Swenson, J. Dynamics of Poly(Ethylene Oxide) around Its Melting Temperature. *Macromolecules* **2013**, *46*, 6949−6954.
(14) Song, S.; Gao, W.; Yang, G.; Zhai, Y.; Yao, J.; Lin, L.; Tang, W.; Hu, N.; Lu, L. Hybrid Poly-Ether/Carbonate Ester Electrolyte Engineering Enables High Oxidative Stability for Quasi-Solid-State Lithium Metal Batteries. *Mater. Today Energy* **2022**, *23*, No. 100893.
(15) Zhai, Y.; Yang, G.; Zeng, Z.; Song, S.; Li, S.; Hu, N.; Tang, W.; Wen, Z.; Lu, L.; Molenda, J. Composite Hybrid Quasi-Solid Electrolyte for High-Energy Lithium Metal Batteries. *ACS Appl. Energy Mater.* **2021**, *4*, 7973−7982.
(16) Polu, A. R.; Rhee, H. W. Ionic Liquid Doped PEO-Based Solid Polymer Electrolytes for Lithium-Ion Polymer Batteries. *Int. J. Hydrogen Energy* **2017**, *42*, 7212−7219.
(17) Xu, F.; Deng, S.; Guo, Q.; Zhou, D.; Yao, X. Quasi-Ionic Liquid Enabling Single-Phase Poly(Vinylidene Fluoride)-Based Polymer Electrolytes for Solid-State LiNi0.6Co0.2Mn0.2O2||Li Batteries with Rigid-Flexible Coupling Interphase. *Small Methods* **2021**, *5*, No. 2100262.
(18) Fenton, D. E.; Parker, J. M.; Wright, P. Complexes of Alkali Metal Ions with Poly(Ethylene Oxide). *Polymer* **1973**, *14*, 589.
(19) Julien, C.; Mauger, A.; Vijh, A.; Zaghib, K. Lithium Batteries. *Lithium Batteries* **2016**, 29−68.
(20) Zhang, W.; Liu, Y.; Guo, Z. Approaching High-Performance Potassium-Ion Batteries via Advanced Design Strategies and Engineering. *Sci. Adv.* **2019**, *5*, No. eaav7412.
(21) Armand, M. B. Polymer Electrolytes. *Annu. Rev. Mater. Sci.* **1986**, 245−261.
(22) Yin, H.; Han, C.; Liu, Q.; Wu, F.; Zhang, F.; Tang, Y. Recent Advances and Perspectives on the Polymer Electrolytes for Sodium/Potassium-Ion Batteries. *Small* **2021**, *17*, No. 2006627.
(23) Stevens, J. R.; Mellander, B. E. Poly(Ethylene Oxide)-Alkali Metal-Silver Halide Salt Systems with High Ionic Conductivity at Room Temperature. *Solid State Ionics* **1986**, *21*, 203−206.
(24) Gao, H.; Xue, L.; Xin, S.; Goodenough, J. B. A High-Energy-Density Potassium Battery with a Polymer-Gel Electrolyte and a Polyaniline Cathode. *Angew. Chem.* **2018**, *130*, 5547−5551.
(25) Zheng, J.; Schkeryantz, L.; Gourdin, G.; Qin, L.; Wu, Y. Single Potassium-Ion Conducting Polymer Electrolytes: Preparation, Ionic Conductivities, and Electrochemical Stability. *ACS Appl. Energy Mater.* **2021**, *4*, 4156−4164.
(26) Fei, H.; Liu, Y.; An, Y.; Xu, X.; Zhang, J.; Xi, B.; Xiong, S.; Feng, J. Safe All-Solid-State Potassium Batteries with Three Dimentional, Flexible and Binder-Free Metal Sulfide Array Electrode. *J. Power Sources* **2019**, *433*, No. 226697.
(27) Fei, H.; Liu, Y.; An, Y.; Xu, X.; Zeng, G.; Tian, Y.; Ci, L.; Xi, B.; Xiong, S.; Feng, J. Stable All-Solid-State Potassium Battery Operating at Room Temperature with a Composite Polymer Electrolyte and a Sustainable Organic Cathode. *J. Power Sources* **2018**, *399*, 294−298.
(28) Armand, M. B.; Bruce, P. G.; Forsyth, M.; Scrosati, B.; Wieczorek, W. Polymer Electrolytes. In *Energy Materials*; John Wiley & Sons, Ltd, 2011; pp 1−31.
(29) Zhang, C.; Xu, Y.; Zhou, M.; Liang, L.; Dong, H.; Wu, M.; Yang, Y.; Lei, Y. Potassium Prussian Blue Nanoparticles: A Low-Cost Cathode Material for Potassium-Ion Batteries. *Adv. Funct. Mater.* **2017**, *27*, No. 1604307.
(30) Eftekhari, A. Potassium Secondary Cell Based on Prussian Blue Cathode. *J. Power Sources* **2004**, *126*, 221−228.

(31) Piernas Muñoz, M. J.; Castillo Martínez, E. Prussian Blue and Its Analogues. Structure, Characterization and Applications. In *SpringerBriefs in Applied Sciences and Technology*; Springer: 2018; pp 9−22.
(32) Lithium, Sodium, Potassium, Rubidium, Caesium and Francium. In *Chemistry of the Elements*, Greenwood, N. N.; Earnshaw, A., Eds.; Butterworth-Heinemann, 1997; pp 68−106.
(33) Bunn, C. W. The Melting Points of Chain Polymers. *J. Polym. Sci.* **1955**, *16*, 323−343.
(34) Kim, Y. W.; Lee, W.; Choi, B. K. Relation between Glass Transition and Melting of PEO−Salt Complexes. *Electrochim. Acta* **2000**, *45*, 1473−1477.
(35) Olmedo-Martínez, J.; Meabe, L.; Basterretxea, A.; Mecerreyes, D.; Müller, A. J. Effect of Chemical Structure and Salt Concentration on the Crystallization and Ionic Conductivity of Aliphatic Polyethers. *Polymers* **2019**, *11*, 452.
(36) Rey, I.; Lassègues, J. C.; Grondin, J.; Servant, L. Infrared and Raman Study of the PEO-LiTFSI Polymer Electrolyte. *Electrochim. Acta* **1998**, *43*, 1505−1510.
(37) Vandeberg, J. T.; Moore, C. E.; Cassaretto, F. P. Vibrational Spectra of Several Potassium Para-Substituted Tetraarylborates. *Spectrochim. Acta, Part A* **1971**, *27*, 501−514.
(38) Sadakane, K.; Fujii, K.; Tsuzuki, S.; Watanabe, H.; Umebayashi, Y. Solvation State of Sodium Tetraphenylborate in 3-Methylpyridine and Its Aqueous Solutions. *J. Mol. Liq.* **2017**, *248*, 53−59.
(39) Bakker, A.; Gejji, S.; Lindgren, J.; Hermansson, K.; Probst, M. M. Contact Ion Pair Formation and Ether Oxygen Coordination in the Polymer Electrolytes M[N(CF3SO2)2]2PEOn for M = Mg, Ca, Sr and Ba. *Polymer* **1995**, *36*, 4371−4378.
(40) Kim, J. H.; Min, B. R.; Won, J.; Kang, Y. S. Analysis of the Glass Transition Behavior of Polymer−Salt Complexes: An Extended Configurational Entropy Model. *J. Phys. Chem. B* **2003**, *107*, 5901−5905.
(41) Huh, P.-H.; Choi, M.-G.; Jo, N. J.; Lee, J.-K.; Lee, J.-O.; Yang, W. Effect of Salt Concentration on the Glass Transition Temperature and Ionic Conductivity of Poly(Ethylene Glycol)-Polyurethane/LiClO4 Complexes. *Macromol. Res.* **2004**, *12*, 422−426.
(42) Aldalur, I.; Martinez-Ibañez, M.; Piszcz, M.; Zhang, H.; Armand, M. Self-Standing Highly Conductive Solid Electrolytes Based on Block Copolymers for Rechargeable All-Solid-State Lithium-Metal Batteries. *Batteries Supercaps* **2018**, *1*, 149−159.
(43) Peters, F.; Langer, F.; Hillen, N.; Koschek, K.; Bardenhagen, I.; Schwenzel, J.; Busse, M. Correlation of Mechanical and Electrical Behavior of Polyethylene Oxide-Based Solid Electrolytes for All-Solid State Lithium-Ion Batteries. *Batteries* **2019**, *5*, 26.
(44) Wu, X.; Jian, Z.; Li, Z.; Ji, X. Prussian White Analogues as Promising Cathode for Non-Aqueous Potassium-Ion Batteries. *Electrochem. Commun.* **2017**, *77*, 54−57.

https://doi.org/10.1021/acsaem.2c01485
ACS Appl. Energy Mater. 2022, 5, 9009−9019